PFC/JA-95-31

The Effects of Field Reversal
on the Alcator C-Mod Divertor

I.H. Hutchinson, B. LaBombard, J.A. Goetz,
B. Lipschultz, G.M. McCracken, J.A. Snipes, J.L. Terry

August, 1995

The Effects of Field Reversal on the Alcator C-Mod Divertor

I.H. Hutchinson, B. LaBombard, J.A. Goetz, B. Lipschultz, G.M. McCracken,
J.A. Snipes, J.L. Terry

Plasma Fusion Center
Massachusetts Institute of Technology
Cambridge, Massachusetts, USA

Abstract

Imbalances between the inboard and outboard legs of the single null divertor in tokamak Alcator C-Mod are observed to reverse when the direction of the toroidal field is reversed. These imbalances are measured by embedded probes in the target plates, tomographic reconstructions of bolometry and line radiation, and visible imaging. Density imbalances of about a factor of ten at the targets are observed at moderate density, decreasing as the density is raised until they are almost balanced. The data indicate that the electron pressure is *not* imbalanced, thus arguing against momentum imbalance as the cause of these drift-induced effects. Instead, power flux imbalance caused by $E_r \wedge B$ convection, and enhanced by radiation, is suggested as the underlying cause.

1. Introduction

In most single null divertor tokamak experiments, imbalance in the heat flux to the inner and outer legs has been observed [1 - 6]. Reversal of the direction of the toroidal field has been shown to alter this imbalance and is accompanied by changes in the amount and location of radiation. These imbalances are of considerable importance for divertor scenarios in which radiative dissipation of the scrape-off-layer (SOL) power is relied upon for mitigating the heat flux to the divertor. If divertor detachment (the reduction of plasma pressure at the targets by neutral momentum effects) is required, then it is essential that both targets should be detached. Imbalances may make this more difficult.

The direction of the toroidal field determines the direction of plasma particle drifts. Therefore, the imbalances that are sensitive to the field direction are almost certainly a reflection of the drifts. In single-null divertors, the "normal" direction of the field is such that $B \wedge \nabla B$ is from the central plasma towards the x-point. This is the configuration that most easily allows attainment of the H-mode confinement regime. For a tokamak with the x-point at the bottom of the vessel, using a right-handed cylindrical coordinate system (R, ϕ, z) of major radius R, toroidal angle ϕ, and height z measured upwards, the sign of the toroidal component of the magnetic field ($B_\phi = B_t$) in the normal configuration is *negative*. The "abnormal" direction has B_t *positive*. (We avoid the use of the term "reversed" field because it tends to imply "negative", leading to easy confusion. We also note that ∇B *never* changes sign. It is always predominantly radially inward.)

In previous experiments it was observed that the power flux to the outboard divertor target tended to exceed that on the inner target by a factor that could exceed 2, for the normal field direction. In the abnormal configuration a more balanced power flux was observed[7]. The radiation characteristics were not so clearly measured but changes of the radiation pattern have definitely been observed. In particular, in DIIID the total power imbalance between the two divertor legs was found to be much less than the target power imbalance because of corresponding imbalance in radiation[8]. Considerable complications in the radiation pattern behavior are associated with detachment and the formation of low temperature "marfes"[9, 10]. Generally, the radiation processes associated with recycling have been observed to be higher in the inboard divertor leg in the normal configuration. In a recent paper, the experimental observations have been reviewed by Chankin *et al* [11].

In Alcator C-Mod, similar characteristics are observed. However, the imbalance is very marked at moderate densities and so offers the opportunity for critical tests of theoretical explanations of the imbalances caused by drifts. Moreover the combination of diagnostics available produces a rather clear picture of the phenomena. In section 2 we describe the diagnostics and show general characteristics of the observed changes in divertor parameters with field direction. Section 3 presents analyses of the database of probe data that show quantitatively the variation of the imbalances with field and density. Section 4 discusses

2

the significance of the measurements for identifying the underlying mechanism. It is shown that the majority of present theoretical approaches are contraindicated by the data. An alternative mechanism is therefore proposed and briefly discussed.

2. Characteristics of Field Reversal

Alcator C-Mod is a compact tokamak, $R = 0.67$ m, $a = 0.21$ m, with high magnetic field[12]. Plasmas have been run at up to 8 T, so far, but most of the results to be reported here are at 5.3 T and have plasma current in the range of 0.6 to 1.0 MA. The safety factor range explored is approximately $3 < q < 5.5$. Elongations between 0.85 and 1.85 have been obtained, but we restrict our attention to $1.6 < \kappa < 1.75$, single-null diverted plasmas, with the x-point in the bottom of the machine. The sign of the toroidal plasma current and the toroidal field are always kept the same as each other because some plasma facing components are designed for only one field-line helicity direction.

For the purposes of comparison of specific discharges, equilibria with negative and positive field were selected that were as similar as possible consistent with the availability of all the critical diagnostics. Detailed comparisons were carried out at moderate core plasma density ($\bar{n}_e = 1. \times 10^{20} \mathrm{m}^{-3}$), and relatively high density ($\bar{n}_e = 2.2 \times 10^{20} \mathrm{m}^{-3}$). Figure 1 shows the negative field equilibrium used for the moderate density case. The positive field equilibrium has small differences in strike-point location on the vertical plates and the upper triangularity of the outermost flux surfaces, but these differences are not significant for the phenomena we are discussing. The equilibria for the high-density comparison were very similar. Reconstruction of the magnetic equilibrium is performed using the EFIT code[13] on the basis of 26 flux and 26 poloidal field measurements at the wall of the vacuum chamber. Poloidal field coil currents and passive eddy currents are accounted for in an axisymmetric approximation. Flux surface locations are found to be reconstructed accurate to about 2 mm in the scrape-off-layer[14].

A wide-angle TV camera views the plasma from the outboard midplane in total visible light. This image is dominated by edge and recycling light and so gives a good impression of the locations of the dominant recycling. Figure 2 shows comparison of two corresponding frames for the negative and positive magnetic field cases. For the normal (negative) direction, the light envelops the inboard divertor plate all the way from the join between the plate and the inboard cylinder down into the deep divertor slot. (Compare with figure 1). No light is easily discernible from the outer divertor. In contrast, for the positive field case, only very faint emission comes from the inboard divertor, with several brighter spots apparently caused by slightly misaligned tiles. Instead the outboard divertor is dominant. However, because the camera can see down into the divertor slot only in those parts of the frame where the view is almost tangential, it is only at those places that the image is bright. Thus, even this rather crude diagnostic shows the very dramatic move of the

recycling light from the inboard to the outboard when the field is changed from negative to positive.

More quantitative analysis of the recycling emission is obtained from tomographic reconstruction of the D_α emission using arrays of filtered visible photodiodes[15]. Four separate arrays view the plasma. One from the top, one from the lower outside looking into the divertor, and two from the outboard. The contributions to the chordal views are calculated from a poloidal map of pixels 2.5 cm square, assuming axisymmetry. Pixel emissivities are calculated that give a linear least squares fit to the chordal data under the constraint of non-negativity and excluding emission from the plasma core or solid areas[15].

Figure 3 shows a smoothed contour plot of the reconstructions for the moderate density case. This is consistent with the TV image in the observation of the location of the emission: on the inboard divertor and extending to the separatrix for the normal field direction, and down in the slot near the outboard strike-point for the abnormal direction. For the higher density case, figure 4 (confirmed by TV images) shows that the effects of reversal are much less dramatic. This is because for both positive and negative fields the brightest recycling light is down in the outboard slot. The outboard emission peak is still about a factor of 2 brighter for the positive field case than for negative field but both are nearly a factor of ten higher than at lower density. The negative field plasma still shows substantial recycling at the inboard divertor, but all these asymmetries are much reduced from the lower density case.

Langmuir probes embedded in the plates are used to give profiles of the plate density and electon temperature[16]. (These are labelled as FMP hereafter.) A fast scanning reciprocating probe (labelled FSP) gives complete profiles of the SOL upstream. Their layout is shown in figure 1. The embedded probes are 3 mm in diameter and domed so that they protrude from the surface by 0.5 mm. This avoids the interpretation problems encountered with flush probes and provides a projected area that is a fairly weak function of field-line angle. Full swept I-V characteristics are used and we observe reasonable exponential behavior in the vicinity of floating potential and below. (Probe data is rejected if exponential fits are not found). The scanning probe has separate Langmuir tips that sample plasma upstream and downstream along the field. Their average current, again using full swept characteristics, is used for determining the density and temperature. Standard interpretation for T_e and n_∞ is used, based on the projected area of the probe along the field direction.

Data from the inboard and outboard targets, and from the scanning probe, is expressed as a function of flux surface, in terms of the distance ρ of the surface outside the separatrix, measured at the outboard midplane. The data from the scanning probe is shifted inward by 2 mm from its nominal ρ value. This once-for-all correction, which is within the uncertainty in the probe position, has been observed to lead to better agreement between upstream and

downstream pressures in the low density cases where pressure balance is expected. The target probe data, on which most of the balance measurements are based, are not shifted. In figure 5 we show plots of three quantities: density, electron temperature, and their product $n_e T_e$, which is the electron pressure, as a function of ρ for the two field directions. The pressure shows rather good agreement between all three curves: FMP inboard, FMP outboard, and fast scanning probe (FSP) over the range $\rho \gtrsim 2$ mm. These are "attached" divertor cases. However, the density and temperature separately show large imbalances. For the normal, negative field case, the temperature at the outboard target is close to that upstream. This is therefore a "sheath-limited" divertor. However, at the same time, the inboard target has very much lower temperature, and very much higher density, by roughly a factor of ten. This is therefore a "conduction-limited" or "high recycling" divertor. With positive field, these asymmetries are reversed. The temperature at the inboard target is higher (although not quite up to the FSP temperature so this is not quite a sheath-limited case) and its density is much lower.

Figure 6 shows the same data for the higher density plasmas. In this case, the temperatures at both targets are low, indicating conduction limited operation. The density is high. There is no longer pressure balance between the targets and the FSP. Instead the targets are detached for $\rho \lesssim 5$mm, which corresponds to the regions on the inboard and outboard that are below the "nose" of the target: on the slightly downward-facing portions of the plate. There is minimal remaining asymmetry in the density between the inboard and outboard targets.

Bolometry reconstructions are obtained from three arrays with a total of twelve chords[17], using an algorithm essentially the same as for the D_α except restricted to the lower divertor area. Figure 7 shows the reconstructed volumetric emissivities for the moderate density case and figure 8 for the high density case. The moderate density case again shows stronger asymmetry changes with field direction. The negative field plasma is dominated by radiation adjacent to the inboard divertor, close to where the D_α is also large, which is also close to the x-point. The positive field plasma has its radiation more on the outboard, although it appears to be higher up, closer to the x-point than the D_α radiation. The higher density case shows some residual asymmetry but both negative and positive field cases have radiation in the vicinity of the x-point, if anything slightly above, with the negative field radiation further inboard, and hence less inside the separatrix than the positive field case.

Quantitative comparison of the powers at the inner and outer targets are shown in table 1. The power to the targets is always a relatively small fraction of the input power but overall power accounting is quite good: to within about 15%. The imbalance of the divertor radiation is able to explain a large fraction of the power imbalance to the target; so that the SOL power imbalance flowing into the divertor does not seem to be very large.

5

Comparing the hydrogenic radiative losses, based on the D_α measurements, with the bolometry, we find that in the moderate density cases the hydrogenic radiation is negligible. In the high density cases we estimate the hydrogenic losses to be up to one quarter of the radiation.

3. Analysis of Database

In order to make the trends already noted more systematic and to perform quantitative comparisons, the Alcator edge database has been analysed for shots relevant to the field direction comparison. Attention has been restricted to ohmically heated shots, almost entirely L-mode, and some shots have been eliminated as having equilibria whose shapes are too different to be relevant. However, with these qualifications, all shots that have appropriate data are included.

Because of the fixed discrete embedded probe positions in the plate, which leads to different ρ positions for different equilibria, a range of ρ is specified. If there is at least one embedded probe on each of the inboard and outboard targets that falls in the specified range then the data qualifies; otherwise it is rejected. Parameters for qualifying shots are then taken to be given by the average of the qualifying probe(s) at either the outboard or inboard, respectively.

Figure 9 shows a plot of the electron temperature at the target versus $\bar{n}_e$ for the four cases in the matrix: positive or negative B_t, inboard or outboard target. The ρ range of 3 - 6 mm is chosen as representative of the bulk of the SOL, not too close to the separatrix, but no more than about one SOL width away. It shows very clearly that the target on the higher-recycling side (inboard negative, outboard positive) is at low temperature over the entire density range. Meanwhile on the lower-recycling side the temperature is high, actually as high as the upstream value, at low $\bar{n}_e$, but falls continuously as density is increased, reaching values close to the higher-recycling side at $\bar{n}_e \gtrsim 1.7 \times 10^{20}$ m^{-3}. There are also asymmetries that are not attributable to drifts, being independent of field direction. The inner plate tends always to be lower in temperature, even when it is the lower-recycling side, than the lower-recycling outboard. However, in our experiments, the asymmetries that are field-direction-dependent predominate.

In figure 10 is plotted the ratio of the outboard to inboard densities for the same shots. The factor of ten in-out asymmetry, which reverses with field direction, is apparent at low density. This disappears as the density is raised. The scatter of the data is fairly significant and attempts have been made to discover correlations with other parameters but with no clear results. In particular, *no* statistically significant variation of the density ratio with safety factor over the range $3 \lesssim q \lesssim 5.5$ is observed. A similar plot to figure 10 but for a lower ρ-range closer to the separatrix shows even more scatter of the data, although the same qualitative trends are clearly present.

In order to obtain as clear a measure as possible of the scaling of the imbalance caused by drifts, we select the low density range ($\bar{n}_e < 1. \times 10^{20}$ m^{-3}) and use an even narrower range of ρ ($2 < \rho < 5$ mm), and plot in figure 11 the density ratio versus the temperature ratio. Two lines are indicated on the plot. The line $(n_{out}/n_{in})(T_{out}/T_{in}) = constant$ corresponds to a situation in which the (electron) pressure is balanced between the inboard and outboard sides. The line $(n_{out}/n_{in})(T_{out}/T_{in})^{3/2} = constant$, on the other hand, correponds to the sheath parallel power flux density being balanced between the inboard and outboard targets. It is clear that a line through the centroids of the positive and negative field points has a slope very close to -1: the balanced pressure case. The balanced power line does not fit the data. Thus our data is evidence that the cause of the field-direction-dependent asymmetries is *not* pressure asymmetries but power asymmetries. This will be discussed further in the next section.

Using the fast scanning probe, we can obtain further evidence of asymmetries by observing the ratio of the ion saturation current to the probe from upstream (the upper part of the plasma) and downstream (the lower divertor). This ratio is indicative of the the parallel ion flow. For this purpose the probe acts as a "Mach Probe". Figure 12 shows this ratio for negative and positive toroidal field. We see that at lower densities, where the field-direction-dependent divertor asymmetries are predominant, a significant asymmetry in flow is evident, giving a saturation current ratio up to nearly 2 that inverts for opposite field direction. A ratio R corresponds to a Mach number of approximately $M = 0.45 \ln R$ [18]; so the maximum observed ratios correspond to $M \approx 0.3$. Flow is in the same direction as the core (ion) plasma current, which, when field line helicity is taken into account, gives rise to a poloidal flow towards the higher-recycling side. In independent measurements based on the observation of plumes produced by local impurity-puffing at the inboard midplane[19], it has nevertheless been established that the parallel flow there is toward the inner divertor regardless of the field direction. Therefore the flow pattern observed by the probe cannot extend all the way round to the inboard midplane, at least for the positive toroidal field plasmas.

4. Mechanism of Divertor Imbalance

In this section we examine the features of candidate mechanisms that might explain the asymmetries observed in our experiments. We do not attempt to model the phenomena quantitatively but we discuss what types of mechanism are consistent with our observations.

Drifts in three possible directions may be important for SOL behavior. These may be conveniently labelled as "radial", "parallel", and "poloidal" refering to the vectorial directions: $\nabla\psi$, $\mathbf{B}$, and $\mathbf{B} \wedge \nabla\psi$, where ψ is the poloidal flux. The "poloidal" drift, under this nomenclature, possesses a small, but ignorable toroidal component. The parallel direction also has a very important component in the poloidal plane. Representative theoretical discussions emphasizing these three different possibilities are, for example, Hinton and Staebler's so-called $\nabla T \wedge \mathbf{B}$ radial drift [20,21], the $\mathbf{E}_r \wedge \mathbf{B}$ poloidal drift discussed, for example, by Tendler and Rozhanskii [22,23], and the parallel momentum diffusion mechanism of Chankin [11]. These are illustrated in figure 13. (The distinction between radial and poloidal drifts is, to some extent artificial, since they both arise from electrostatic forces crossed with the field. Nevertheless, a distinction may be helpful for understanding the mechanisms.)

A second classification of causes of drift-dependent divertor asymmetries seems equally important. That is, whether the asymmetries arise from pressure asymmetry or from power asymmetry. The predominant tendency so far in trying to explain divertor asymmetries has been to do so in terms of pressure asymmetries. This has not been fully explicit in many treatments. However, the underlying rationale has been the intuition that density asymmetries are to be explained by preferential particle drifts *towards* the region of higher observed density.

This intuition is erroneous for cross-field drifts. The connection of the inboard and outboard regions along the field means that imbalance in the pressure would require a parallel momentum source along the field line. Such a source might come from viscous momentum transport acting on a parallel SOL outflow arising in response to a perpendicular inflow. However, if the perpendicular diffusivity of parallel momentum is comparable to the particle diffusivity, then appreciable pressure imbalance requires the parallel flow to be a substantial fraction of the sound speed over much of the SOL. Moreover, it would mean that the parallel flow would be away from the higher density region, opposite to what is observed on Alcator.

Power asymmetries, however, can arise from convection associated with drifts, without the same pressure constraints. Moreover, these asymmetries will in general be opposite to the intuition mentioned above. That is, the density will be higher at the side with lower power flux. For this reason, the convective power flux attributable to particle drifts

tends to lower the density in the region towards which they flow. This statement may be understood very simply as follows.

The parallel power density, $q_\parallel$, to the divertor target is equated to the sheath power flux, normally written $0.5\gamma n_t T_t (2T_t/m_i)^{1/2}$, where subscript t refers to the target, the sound-speed has been taken to involve $T_e + T_i = 2T_t$, and γ is the sheath power transmission factor, usually ~ 8. Therefore we can write:

$$T_t = \frac{m_i}{2}\left(\frac{q_\parallel}{0.5\gamma n_t T_t}\right)^2 \qquad \text{and} \qquad n_t = \frac{2}{m_i}\left(\frac{0.5\gamma}{q_\parallel}\right)^2 (n_t T_t)^3 \quad .$$

Applying these equations to the opposite ends of a flux tube, on the outboard and inboard targets, subscripts 1 and 2, assuming γ is the same, one trivially finds:

$$\frac{T_{t1}}{T_{t2}} = \left(\frac{q_{\parallel 1}}{q_{\parallel 2}}\right)^2 \left(\frac{n_{t2}T_{t2}}{n_{t1}T_{t1}}\right)^2 \qquad \text{and} \qquad \frac{n_{t1}}{n_{t2}} = \left(\frac{q_{\parallel 2}}{q_{\parallel 1}}\right)^2 \left(\frac{n_{t1}T_{t1}}{n_{t2}T_{t2}}\right)^3 \quad .$$

Thus, power ($q_\parallel$) asymmetries act in the opposite direction to pressure ($n_t T_t$) asymmetries.

Our measurements, especially figure 11, indicate that the dominant asymmetry is in fact power, not pressure. Therefore, in seeking an explanation in terms of drifts we must look for drift, and corresponding convective heat flow, that is *away from* the higher recycling side. This immediately indicates which of the drifts is the likely explanation. As discussed by Chankin[11] for example, and illustrated in figure 13, the radial drifts of Hinton and Staebler are towards the high recycling side, while the poloidal $\mathbf{E}_r \wedge \mathbf{B}$ drifts are away from the high recycling side. Contrary to most previous authors' discussion, we therefore *reject* the radial drift and *accept* the poloidal $\mathbf{E}_r \wedge \mathbf{B}$ drifts as candidates for explaining our data.

The parallel momentum mechanism of Chankin, would give a force on the SOL in the same direction as the observed parallel flows. However, our observed pressure balance, which is in contradiction with the JET interpretation[24], is evidence against this mechanism.

Focussing, then on the $\mathbf{E}_r \wedge \mathbf{B}$ drift, we examine whether it is large enough to be significant. The radial electric field is regarded as arising from the difference in sheath potential drop between the plasma upstream and the equipotential divertor target, when an electron temperature difference exists along the plate. Therefore the magnitude of the electric field is estimated to be

$$\mathbf{E}_r \approx -C\nabla T_t/e \quad ,$$

where the coefficient, C, governing the sheath potential drop, depends to some extent on the collisionality and the field line angle on the target, but is typically between 1 and 3, and the temperatures are those at the target (traced along the flux tube from the point in

question, ignoring resistive potential drops). If the temperature scale length derived from T_t is $\lambda_T \equiv T_t/(dT_t/d\rho)$, the poloidal drift velocity at the midplane, where ρ is measured, is then $CT_t/(\lambda_T eB)$. The parallel heat flux is taken to be represented by its value at the target. Then, comparing the convective heat flux arising from the drift to the poloidal component of the parallel heat-flux, we obtain the ratio, R_d of the convective drift heat flux to the parallel heat flux as

$$R_d = \frac{CT_t 5n_t T_t}{\lambda_T eB} \frac{1}{0.5\gamma n_t T_t (2T_t/m_i)^{1/2}} \frac{B}{B_p} = \frac{5C}{\gamma} \frac{\rho_s}{\lambda_T}$$

where $5n_t T_t$ is the energy density being convected at the $\mathbf{E}_r \wedge \mathbf{B}$ velocity assuming pressure balance and equal electron and ion temperatures, and $\rho_s \equiv (2m_i T_t)^{1/2}/(eB_p)$ is the poloidal ion gyro radius based on the sound speed, measured at the target temperature. The coefficient $5C/\gamma$ is of order unity. Obviously, when there is strong temperature imbalance, as in our experiments, the assumption of negligible resistive potential drop is a poor approximation, since the potentials at the sheath edge are different on either side. In such a situation, it seems likely that the hotter side will predominate in setting the SOL potential.

Quantitatively, the midplane poloidal field in these Alcator C-Mod discharges is approximately 0.6 T, and λ_T is of order 0.005 m (although varying with T_e [16]). Therefore for temperature 10 eV, we find $\rho_s \sim 1$ mm and $R_d \approx \rho_s/\lambda_T \sim 0.2$. For the lower density range, the target temperature reaches about 30 eV, which would give $R_d \approx 0.35$. The power imbalance arising from this effect alone would then be $1.35/0.65 = 2.08$, which would give rise to a density ratio of over 4. When enhanced by radiation, this seems more than enough to account for the observations. As shown in table 1, radiative loss is higher on the higher density (lower sheath power) side and enhances the power imbalance and consequently the density imbalance. The radiative loss imbalance nevertheless must be triggered by a drift effect, which we suggest may be the convective heat flux imbalance.

Our rough estimate shows that $\mathbf{E}_r \wedge \mathbf{B}$ drift convective heat flux is of the right order of magnitude to explain the observed imbalances. Direct control of this drift through divertor biassing in Tokamak de Varennes has been observed [25] to raise the total heat-flux into the chamber towards which the drift is directed. It should be noted, however, that we are implicitly assuming that the $\mathbf{E}_r \wedge \mathbf{B}$ drift requires extra power to be carried through the sheath in the form $0.5\gamma n_t T_t (2T_t/m_i)^{1/2}$. The effect of the drift in altering this formula has been ignored. Therefore more detailed theory of the drift effects on the sheath is clearly necessary [26,27].

Moreover, the theoretical ratio of drift to target heat flux is proportional to $T_t^{1/2}$, for constant λ_T. Therefore the observation that the imbalance decreases as the hotter target temperature decreases, appears consistent with this interpretation. In contrast,

for example, the radial $\nabla T \wedge B$ drift might be expected to increase as the temperature difference between upstream and the target is increased by a fall of the target temperature.

The observed direction of the parallel flow (out of the divertor towards which the poloidal drifts flow) is what would be necessary to balance the drift inflow. However, we must presume that the balance is incomplete. Otherwise the convective power from the parallel flow would also cancel that from the drift and the power asymmetry would disappear. Once again, a more complete, self-consistent model is needed.

5. Summary

Very strong imbalances in divertor target density and temperature that reverse with the sign of the toroidal field have been measured on Alcator C-Mod. Recycling and radiative power loss are concentrated on the high density, low temperature side. The imbalances are largest at the lowest line-average density studied (0.5×10^{20} m^{-3}) and decrease rapidly with increasing density, as the hotter side cools, till (above about 1.7×10^{20} m^{-3}) they are within experimental scatter. Parallel flow that reverses with field direction, with Mach number up to 0.3 at low density, has been observed, and likewise decreases to small levels as the density rises.

At the lower densities, where the imbalance is large enough to detect the difference between pressure imbalance and power imbalance, the measurements indicate that pressure is not imbalanced but that power is. This argues against many of the current theories of the origin of the observed field-direction-dependent divertor imbalances, based on pressure asymmetry. The convective heat flux carried by the poloidal $E_r \wedge B$ drift is the mechanism we suggest as the cause of the asymmetries. It has the right direction, the right order of magnitude and the right dependence on density, through the electron temperature at the plate. It is also a source of power imbalance, as required by the measurements, and its particle flows are consistent with the measured parallel particle flows.

The effects of imbalanced radiation enhance the power imbalance, and indeed largely account for the final state. We cannot rule out the possibility that impurity-fraction imbalance is significant, but the density and temperature imbalances are probably sufficient to account, on their own, for the radiation imbalance.

References.

[1] Wagner F, Keilhacker M and the ASDEX and NI Teams 1984 *J. Nucl. Mater.* **121** 103

[2] Harbour P J 1988 *Contrib. Plasma Phys.* **28** 4/5 417

[3] Nakazawa I *et al* 1989 *Proc. 16th Eur. Conf. on Controlled Fusion and Plasma Phys. (Venice, 1989)* vol 13B, part 3, p 887

[4] Hill D N *et al* 1990 *J. Nucl. Mater.* **176&177** 158

[5] Reichle R *et al* 1991 *Proc. 18th Eur. Conf. on Controlled Fusion and Plasma Phys. (Berlin, 1991)* vol. 15C, part 3, p 105

[6] Itami K, Shimada M and Hosogane N 1992 *J. Nucl. Mater.* **196&198** 755

[7] Janeschitz G *et al* 1993 *Proc. 20th Eur. Conf. on Controlled Fusion and Plasma Phys. (Lisboa, 1993)* vol. 17C, part 2, p 559

[8] Leonard A W, Lasnier C J, Cuthbertson J W, Evans T E, Fenstermacher M E, Hill D N, Jong R A, Meyer W H, Petrie T W, Porter G D 1995 *J. of Nucl. Mater.* **220-222** 325

[9] Asakura N, Itami K, Hosogane N, Tsuji S, Shimizu K, Kubo H, Sugie T, Takizuka T and Shimada M 1995 *J. of Nucl. Mater.* **220-222** 395

[10] Asakura N, Shimizu K, Hosogane N, Itami K, Tsuji S and Shimada M *et al* 1995 *Nucl. Fusion* **35** 381

[11] Chankin A V *et al* 1994 *Plasma Phys. Controlled Fusion* **36** 1853

[12] Hutchinson I H *et al* 1994 *Phys. Plasmas* **1** 1511

[13] Lao L L, St. John H, Stambaugh R D, Kellman A G and Pfeiffer W 1985 *Nucl. Fusion* **25** 1611

[14] Hutchinson I H, Horne S, Tinios G, Wolfe S M and Granetz R S 1995 PFC Report PFC/JA-95-4 *submitted to Fusion Technology*

[15] Kurz C, Snipes J A, Terry J L, LaBombard B and McCracken G M 1995 *Rev. Sci. Instrum.* **66 (1)** 619

[16] LaBombard B *et al* 1995 *Phys. Plasmas* **2** 2242

[17] Goetz J A, Lipschultz B, Graf M A, Kurz C, Nachtrieb R, Snipes J A, Terry J L 1995 *J. Nucl. Mater.* **220-222** 971

[18] Hutchinson I H 1988 *Phys. Rev. A* **37** 4358

[19] Jablonski *et al* private communication.

[20] Hinton F L and Staebler G M 1989 *Nucl. Fusion* **29** 405

[21] Staebler G M 1991 *Nucl. Fusion* **31** 729

[22] Tendler M and Rozhansky V 1990 *Comments Plasma Phys. Controlled Fusion* **13** 191

[23] Tendler M and Rozhansky V 1992 *J. Nucl. Mater.* **196-198** 912 Comments Plasma Phys. Controlled

[24] Chankin A V, Clement S, deKock L, Erents S K, Harbour P J, and Tagle J A 1992 *J. Nucl. Mater.* **196-198** 739

[25] Décoste R, *et al* 1994 *Phys. Plasmas* **1** 1497

[26] Chankin A V and Stangeby P C 1994 *Plasma Phys. Control. Fusion* **36** 1485

[27] Stangeby P C and Chankin A V 1995 *Phys. Plasmas* **2** 707

Table 1. The power balance for the four characteristic plasmas. The total (ohmic) input power in MW is compared with bolometric measurements of the power loss from the main chamber, the x-point inside the separatrix, the inner and outer divertor legs. The power to the inner and outer targets is estimated from the Langmuir probe profiles where sufficient data is available, using a power transmission factor of $\gamma = 7$.

$n_e/10^{20}\mathrm{m}^{-3}$	Field	Input	Main	x-point	Outer leg	Inner leg	Outer target	Inner target
0.8	−	0.88	0.21	0.04	0.13	0.28	0.20	0.03
0.7	+	1.06	0.28	0.11	0.33	0.15	0.10	0.05
1.8	−	1.26	0.51	0.17	0.24	0.24	0.14	0.02
1.8	+	1.24	0.65	0.18	0.23	0.19	0.09	−

Figure Captions.

Figure 1. Equilibrium used in comparison of negative and positive toroidal field plasmas. The probes embedded in the inner and outer divertor targets and the rapid-scan reciprocating probe are also shown.

Figure 2. Comparison of wide-angle TV images of the lower divertor region in total visible light, with toroidal field (a) negative, (b) positive. Camera settings and exposure are identical. The intense recycling light envelops the inner divertor up as far as the inner cylinder for negative toroidal field. In contrast, for positive field, the inner divertor is dim and the brightest chord is that which looks almost tangentially into the divertor slot.

Figure 3. Tomographic reconstructions of the D_α emission from the diode arrays. Plasma current 0.8 MA., line average density $\bar{n}_e \approx 0.8 \times 10^{20} \mathrm{m}^{-3}$. Toroidal field (a) negative, (b) positive.

Figure 4. Tomographic reconstructions of the D_α emission from the diode arrays. Plasma current 0.8 MA, line average density $\bar{n}_e \approx 1.8 \times 10^{20} \mathrm{m}^{-3}$. Toroidal field (a) negative, (b) positive.

Figure 5. Probe profiles for the moderate density case (figure 3). Toroidal field (i) negative, (ii) positive. Profiles of density (a), temperature (b), and electron pressure (c).

Figure 6. Probe profiles for the high density case (figure 3). Toroidal field (i) negative, (ii) positive. Profiles of density (a), temperature (b), and electron pressure (c).

Figure 7. Radiative loss tomographic reconstructions for the moderate density plasmas of figure 3. (a) negative, (b) positive toroidal field.

Figure 8. Radiative loss tomographic reconstructions for the high density plasmas of figure 3. (a) negative, (b) positive toroidal field.

Figure 9. Mean temperature in the range $0.003 < \rho < 0.006$ versus line-average density.

Figure 10. Ratio of the density at the outboard target to that at the inboard target on the same flux surface versus line average density.

Figure 11. The outboard/inboard density ratio versus temperature ratio for shots with density less than $1.10^{20} \mathrm{m}^{-3}$, compared with the theoretical ratio dependence for balanced pressure or power.

Figure 12. Ratio of the ion saturation currents to the upstream and downstream collectors of the reciprocating probe. Positive ratio of upstream to downstream indicates parallel

flow with positive toroidal component. The poloidal component of such a parallel flow is towards the outboard divertor.

Figure 13. Schematic illustration of the drifts anticipated for negative toroidal field.

Fig 1

B negative

B positive

Fig 2

negative B

(a)

positive B

(b)

Fig 3

negative B

(a)

60 kW-m⁻³
50
40
30
20
10

positive B

(b)

60 kW-m⁻³
50
40
30
20
10

Fig 4

5 (a)

5 (b)

5 (c)

6 (a)

6 (b)

6 (c)

negative B

positive B

Fig 7

negative B

positive B
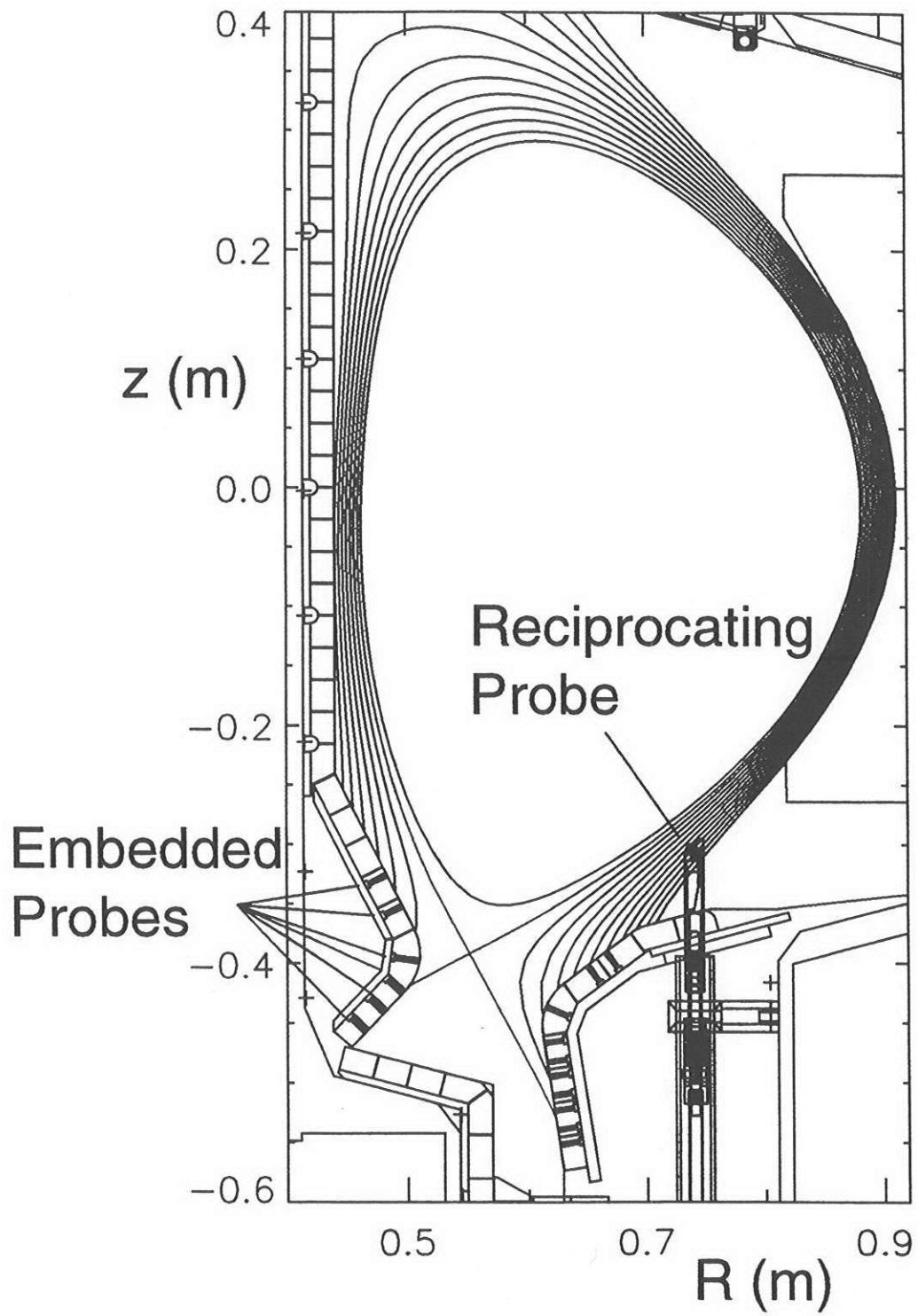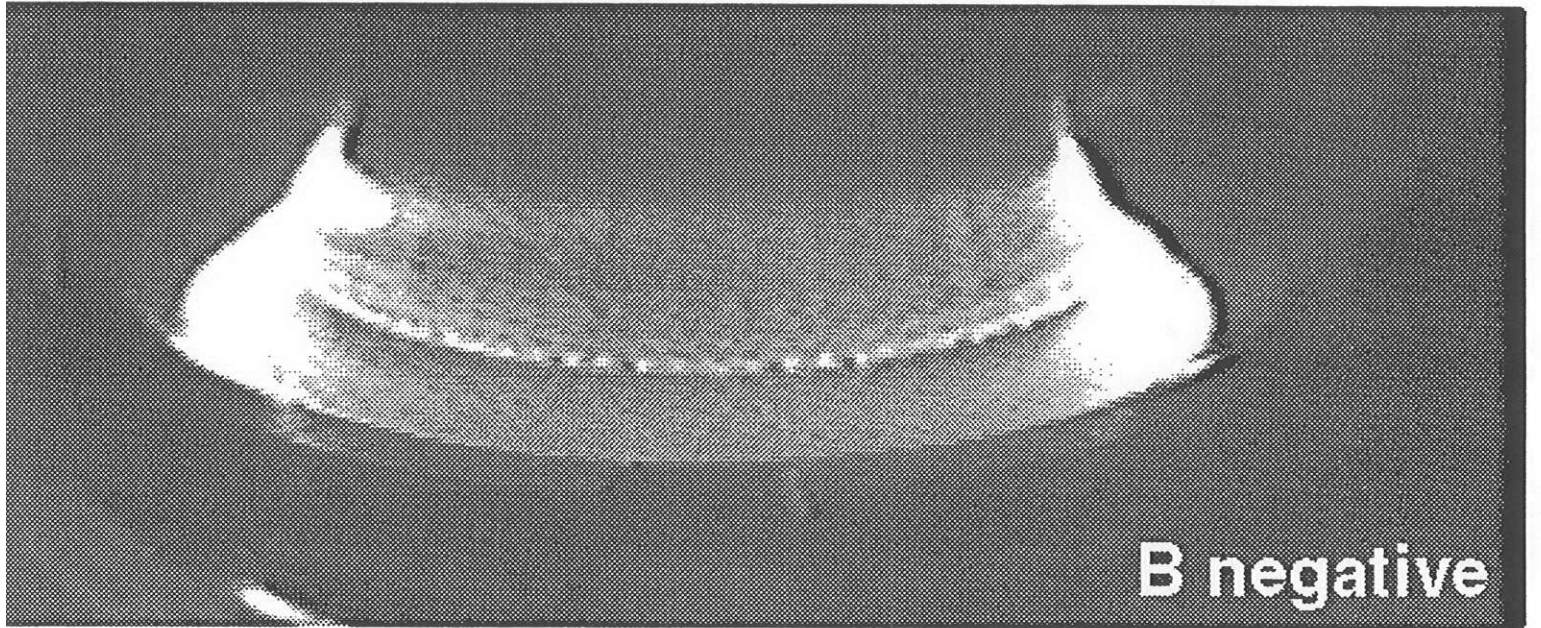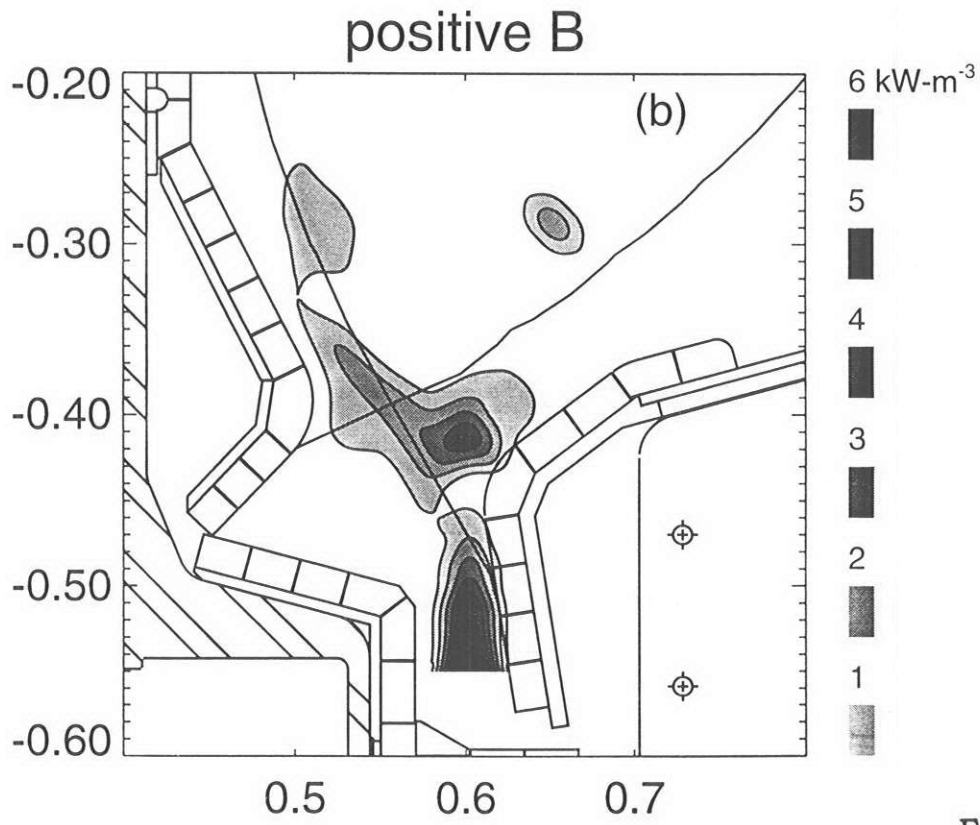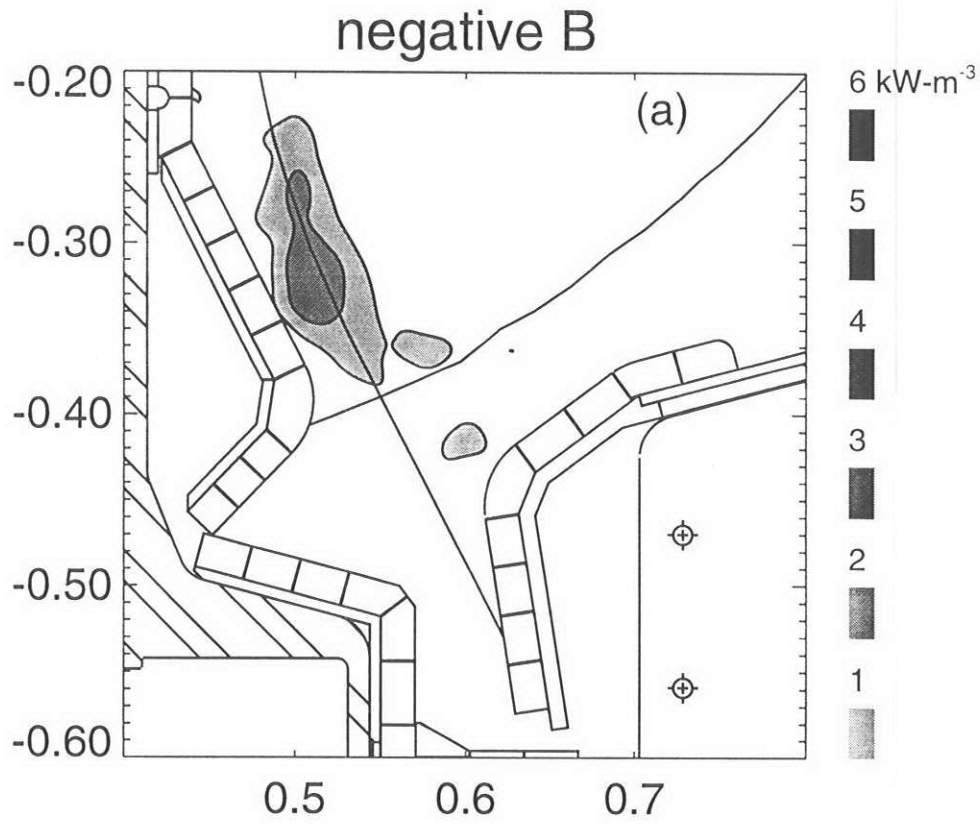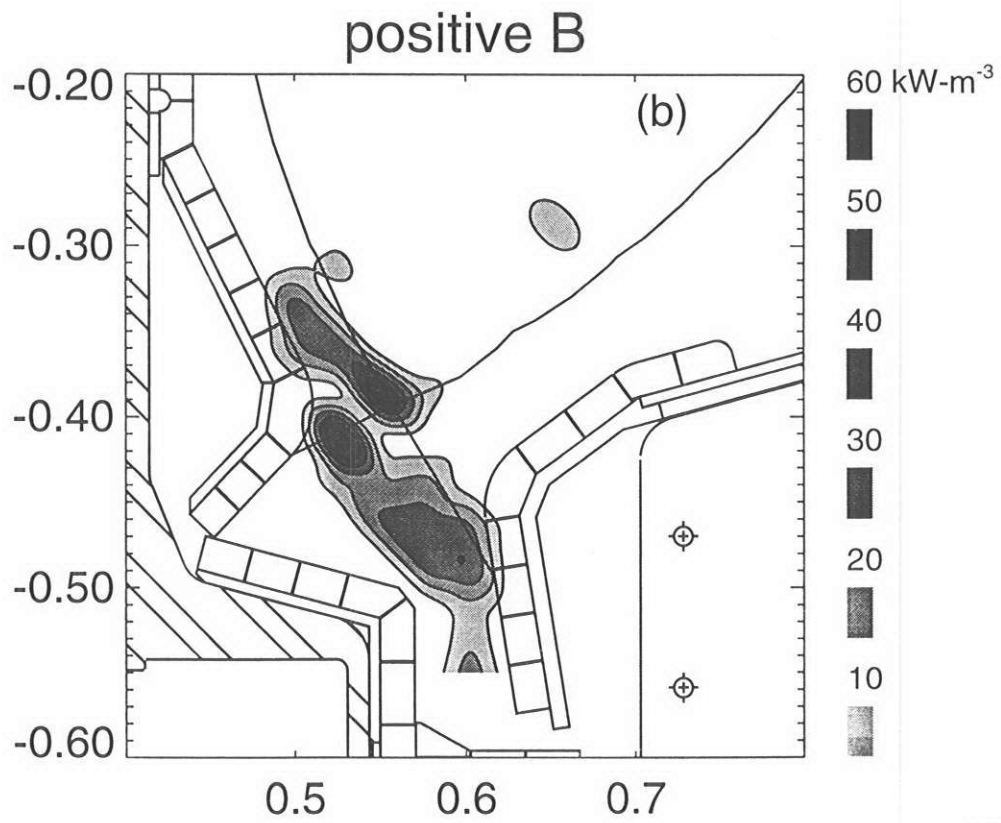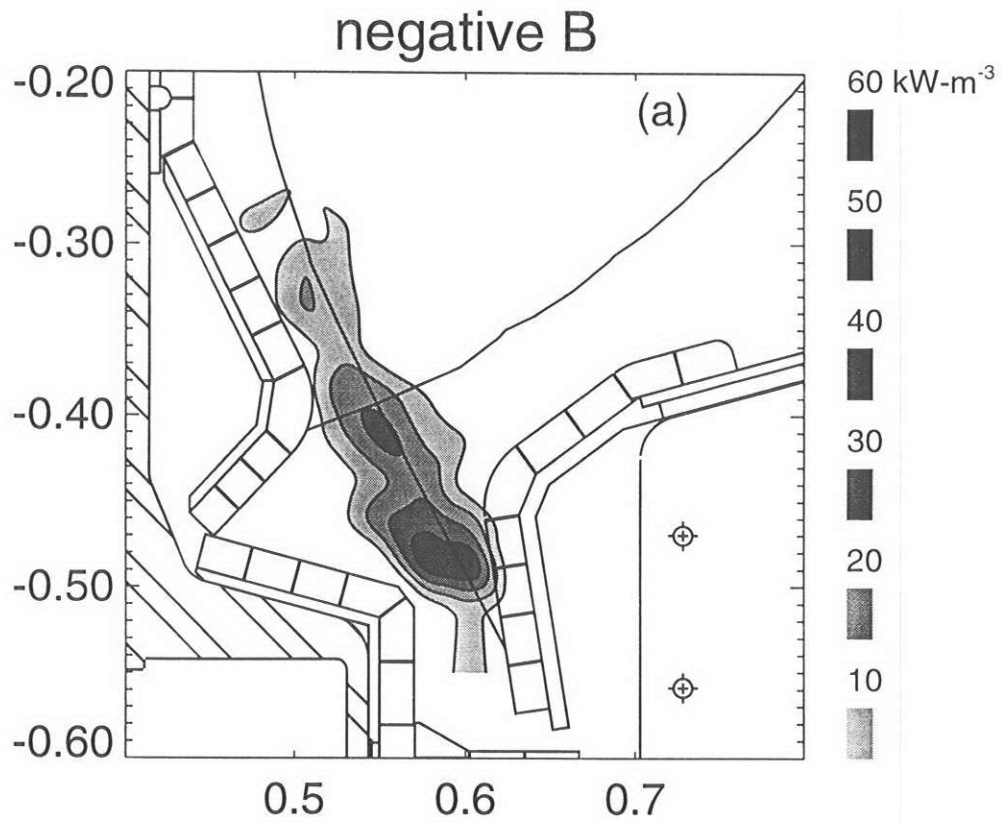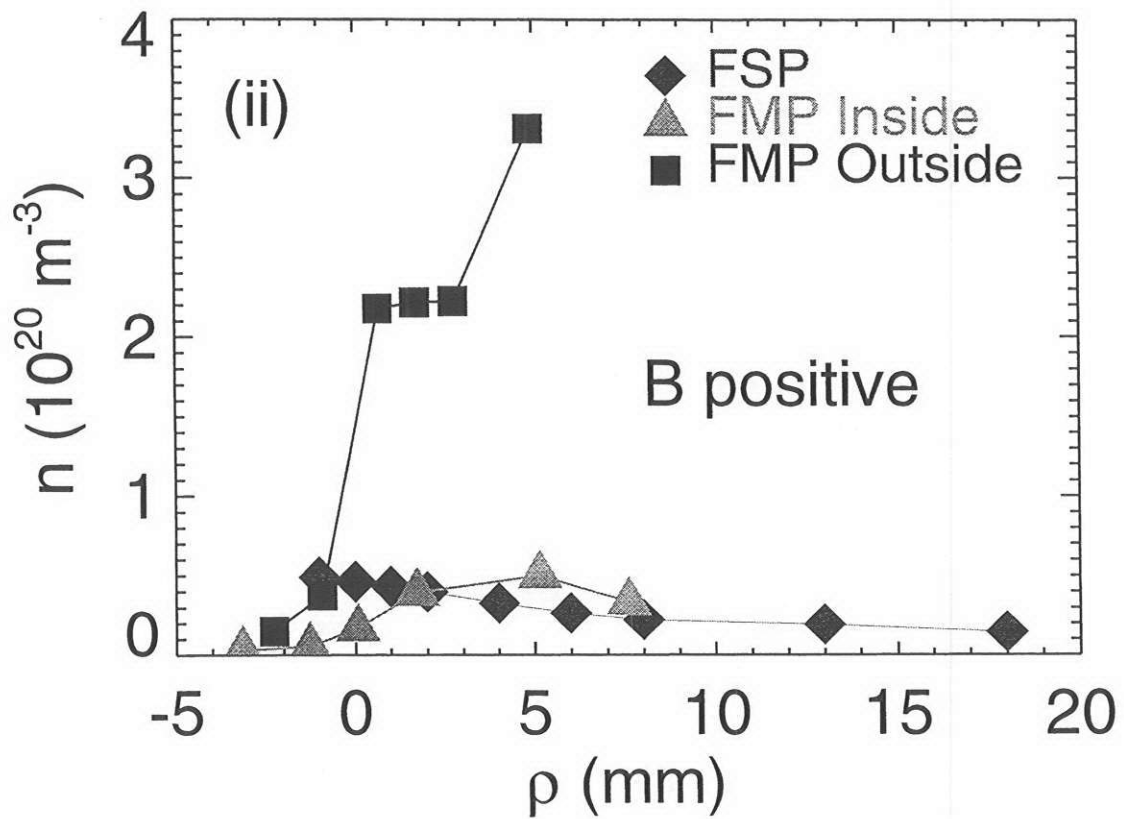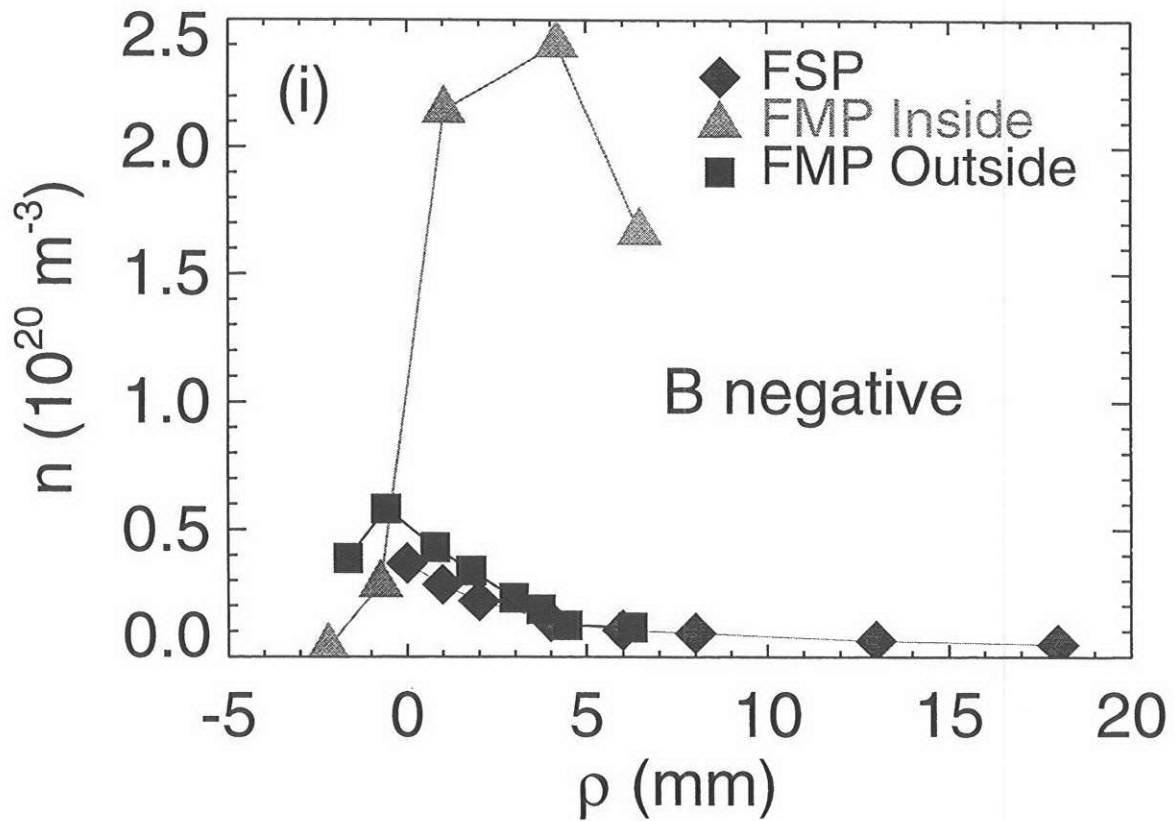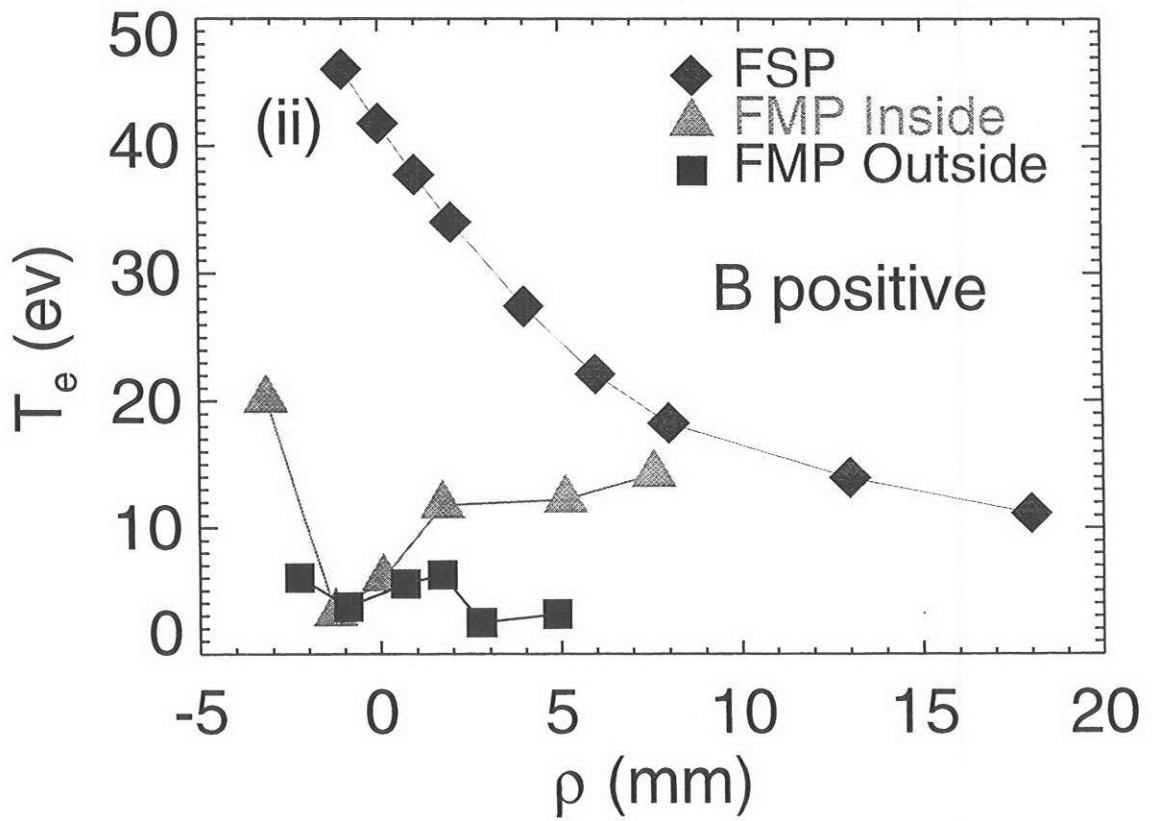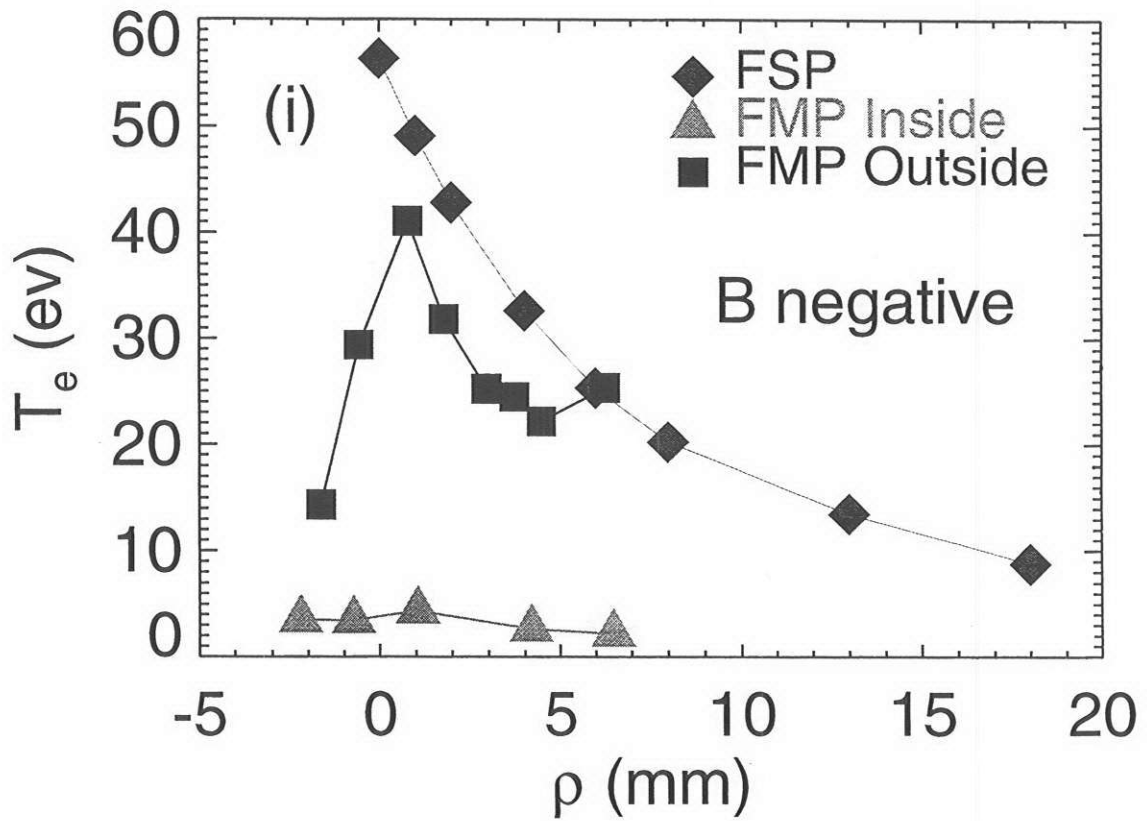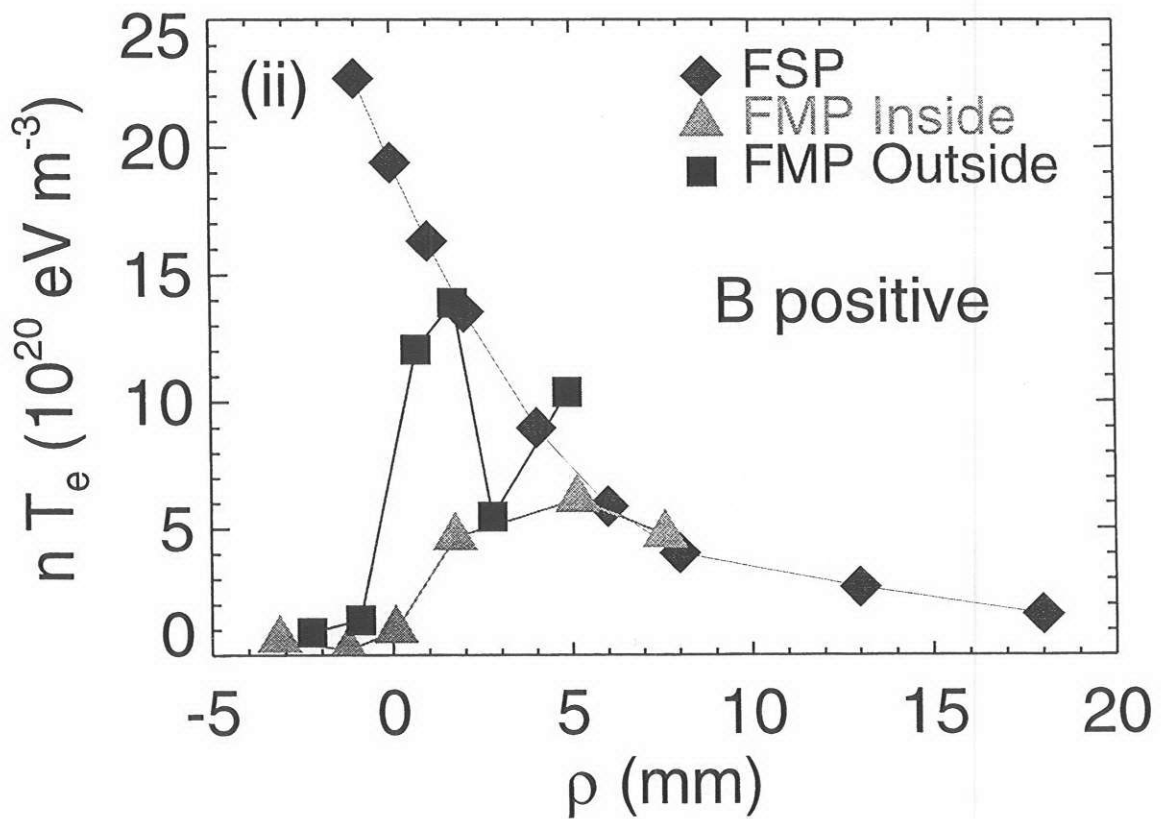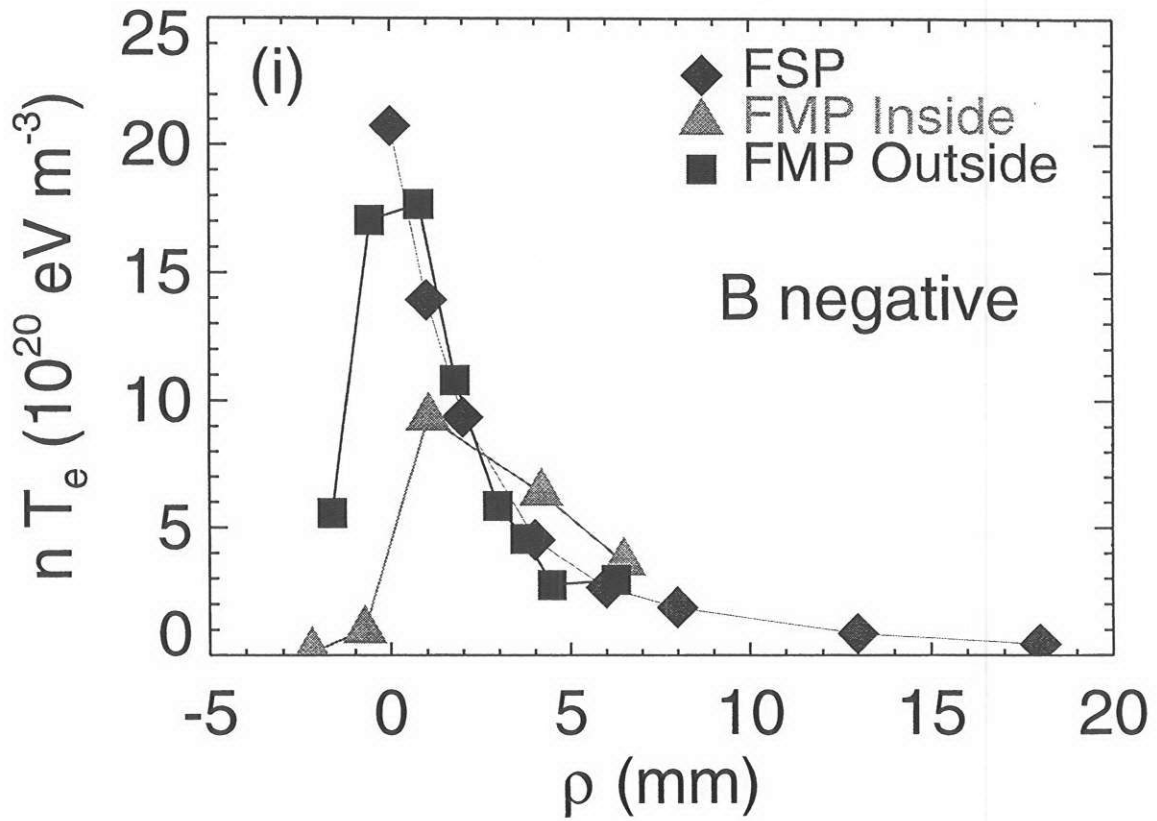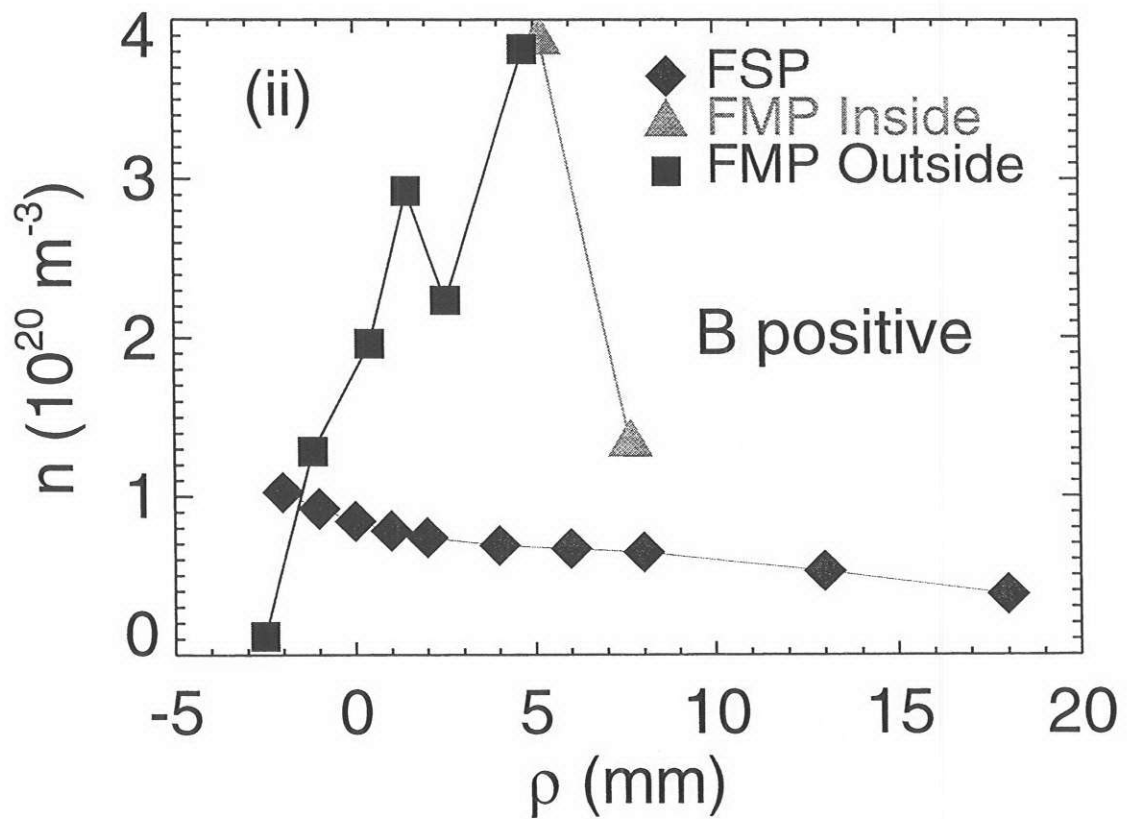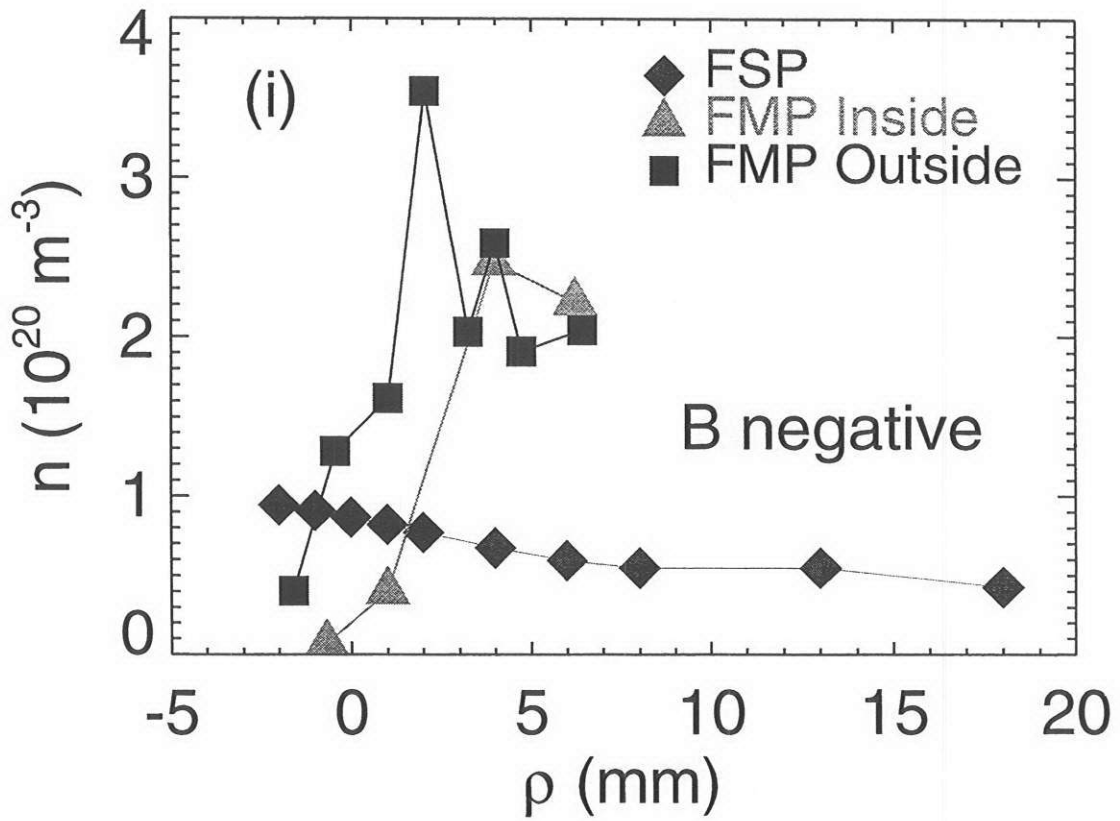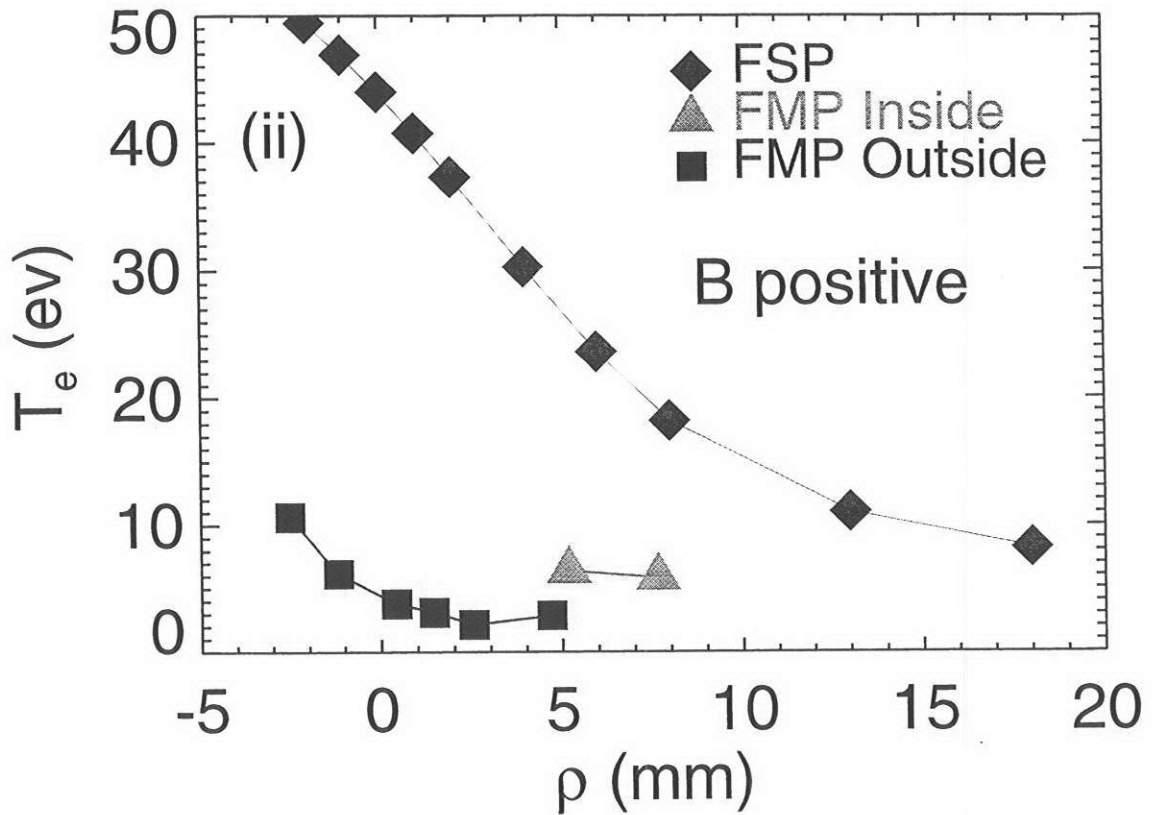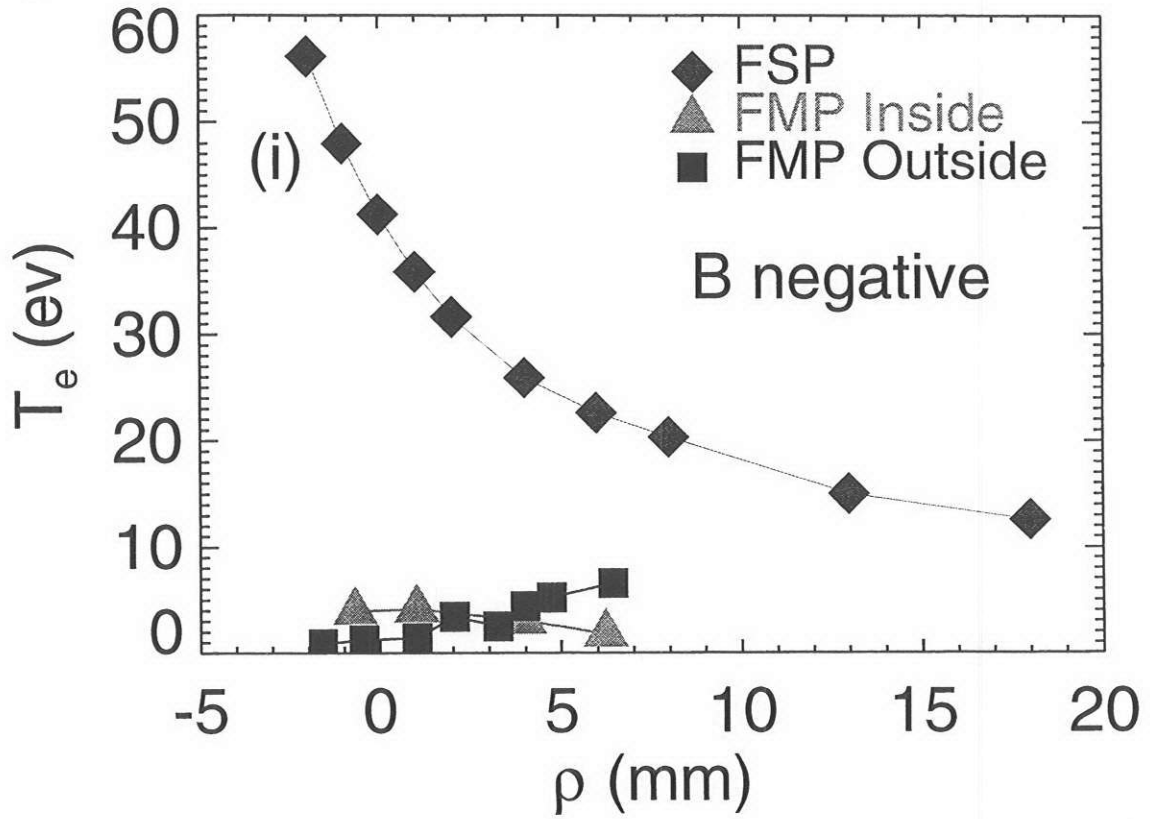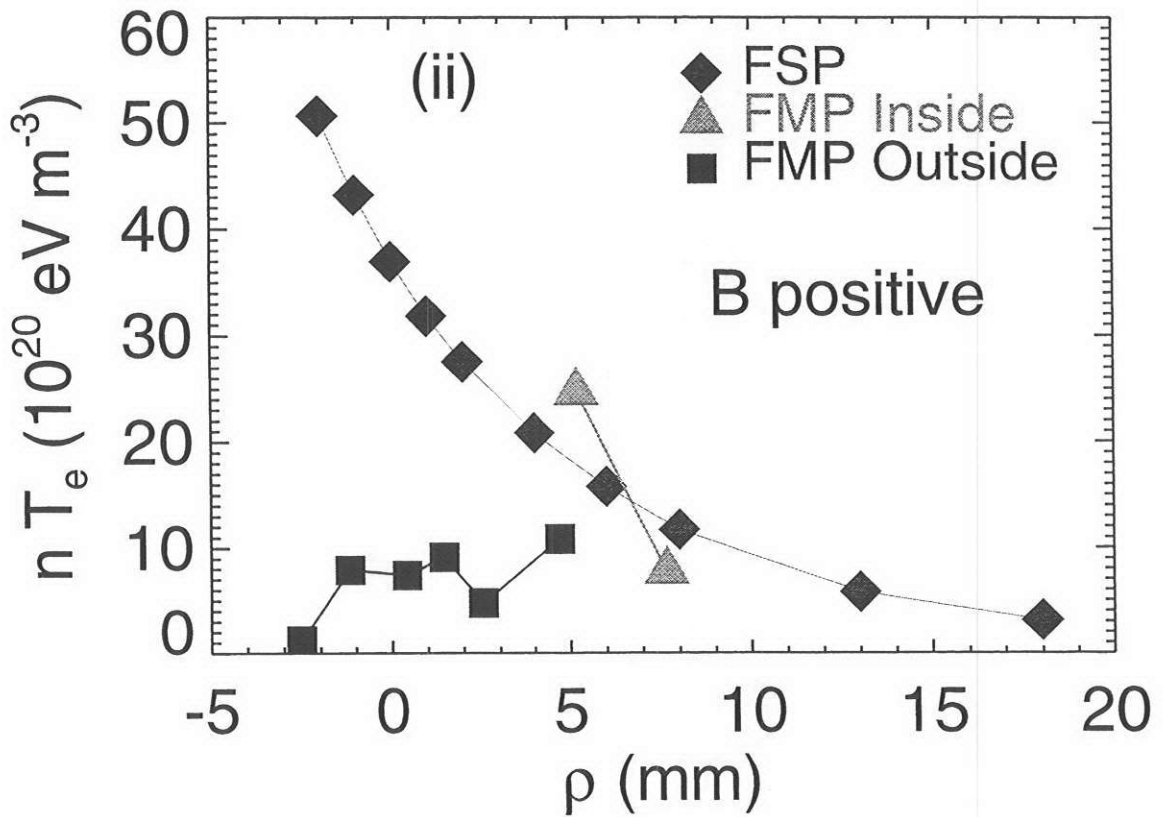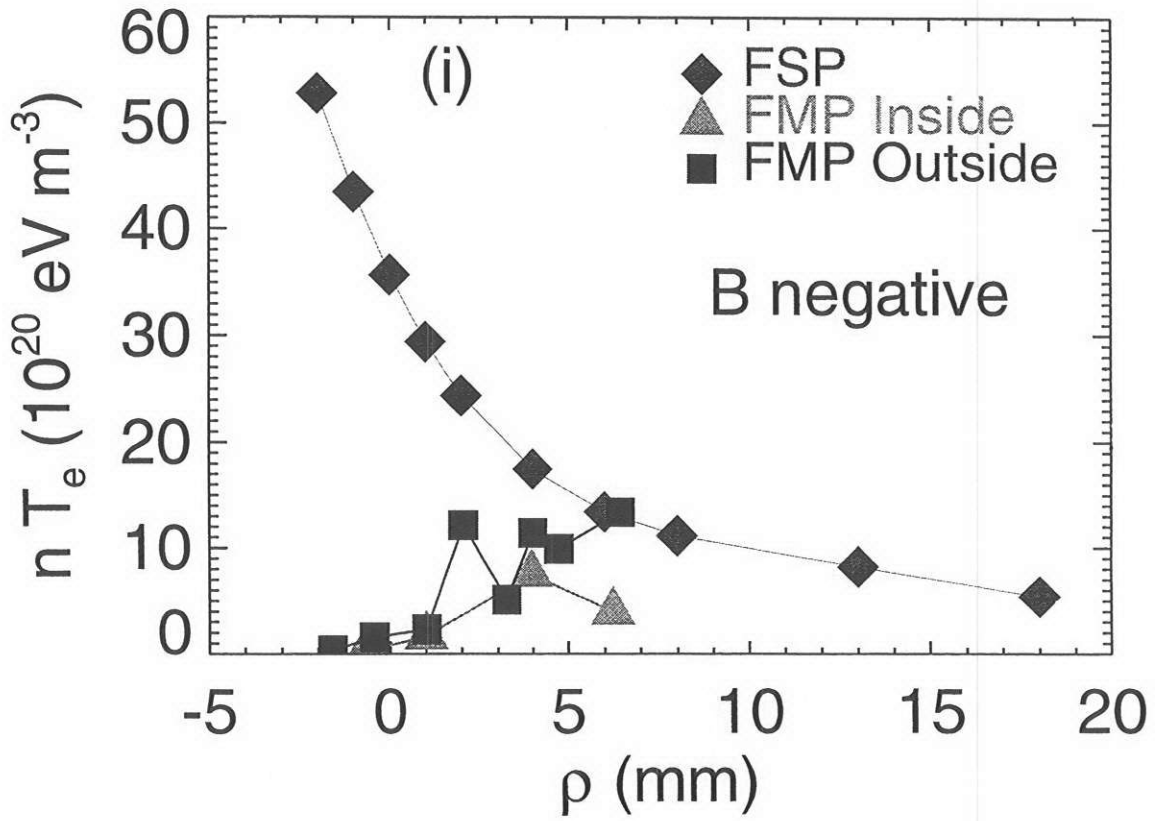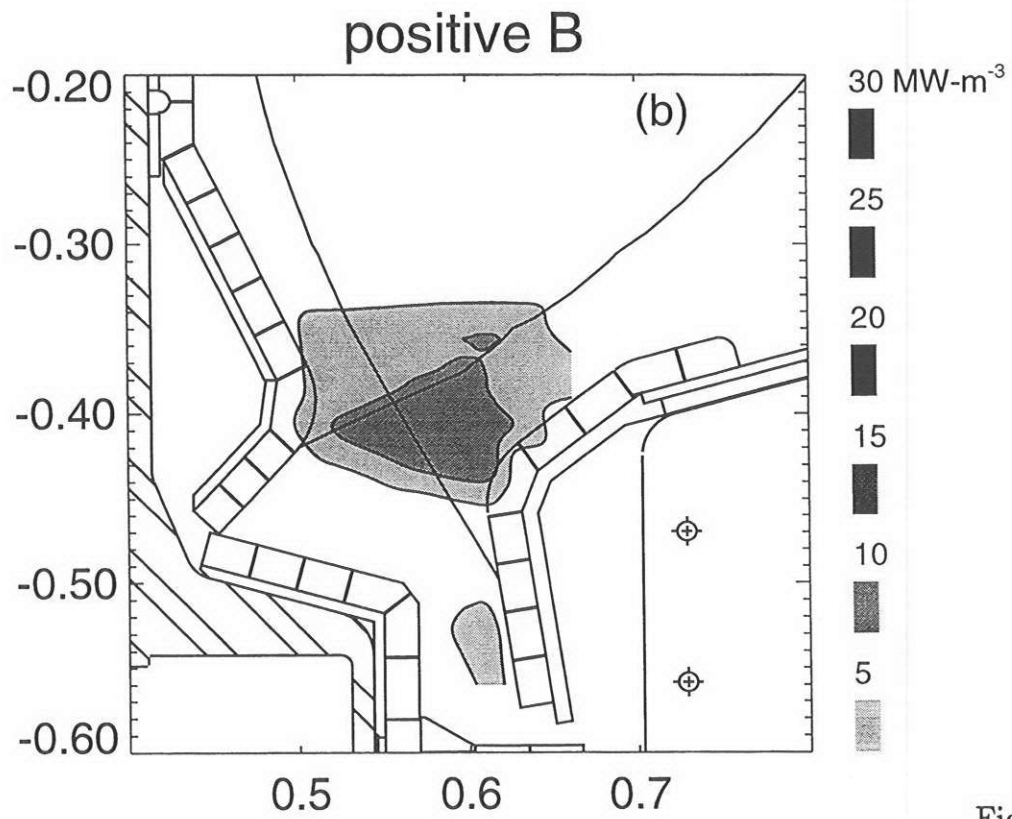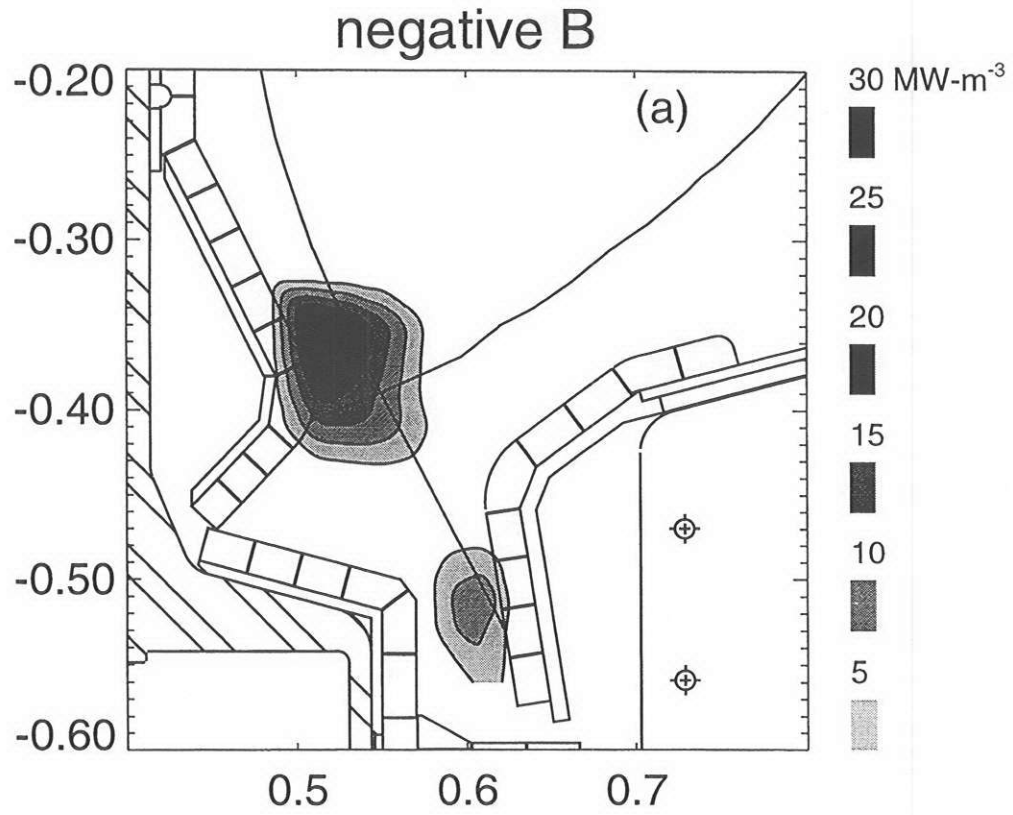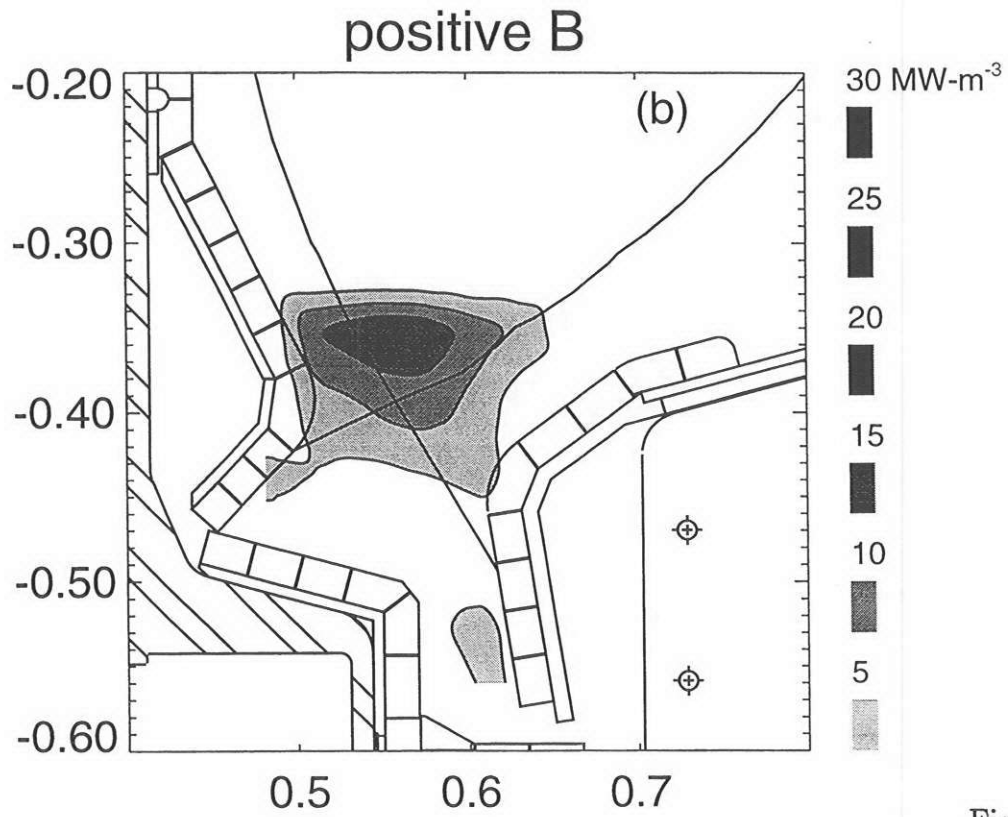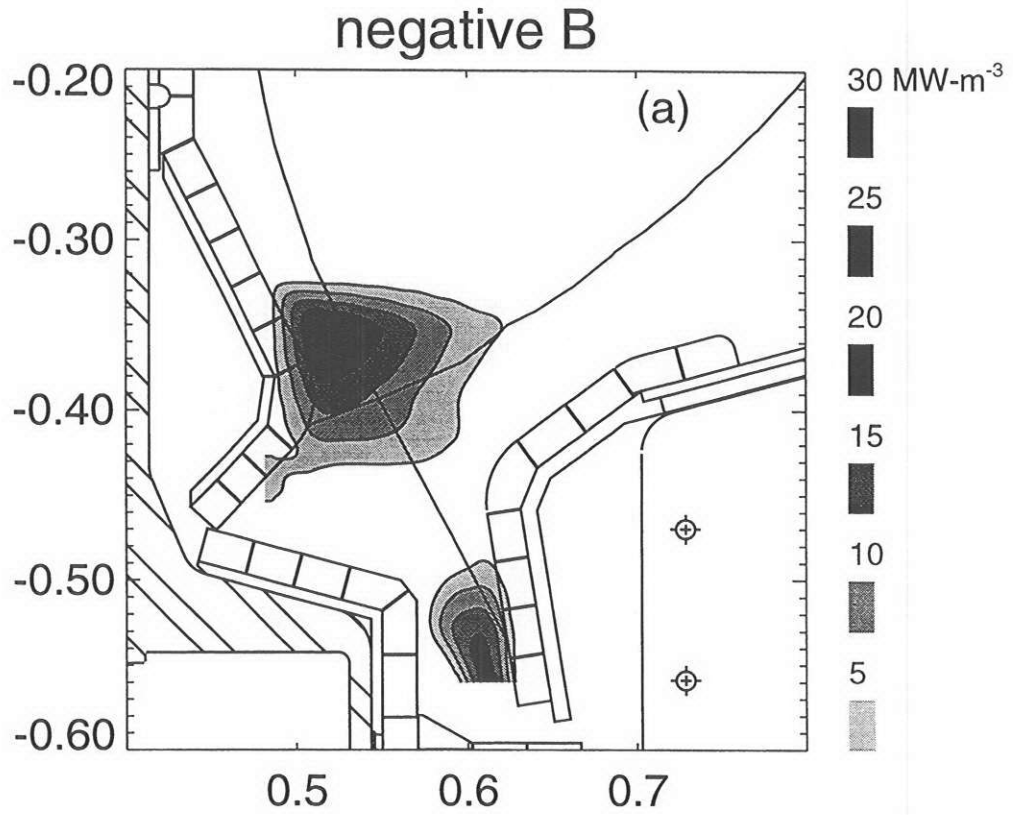
Fig 8
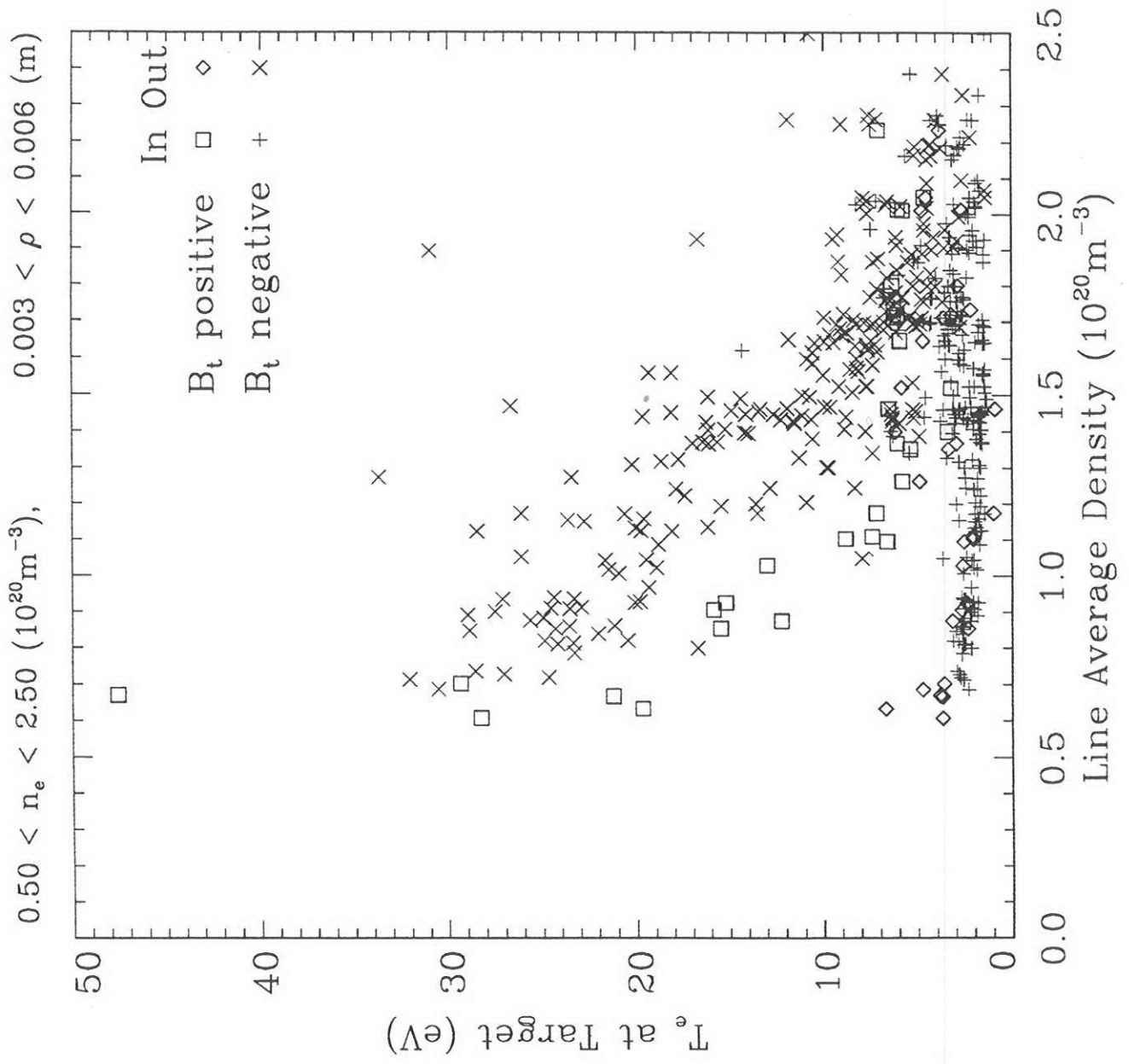
Fig 9
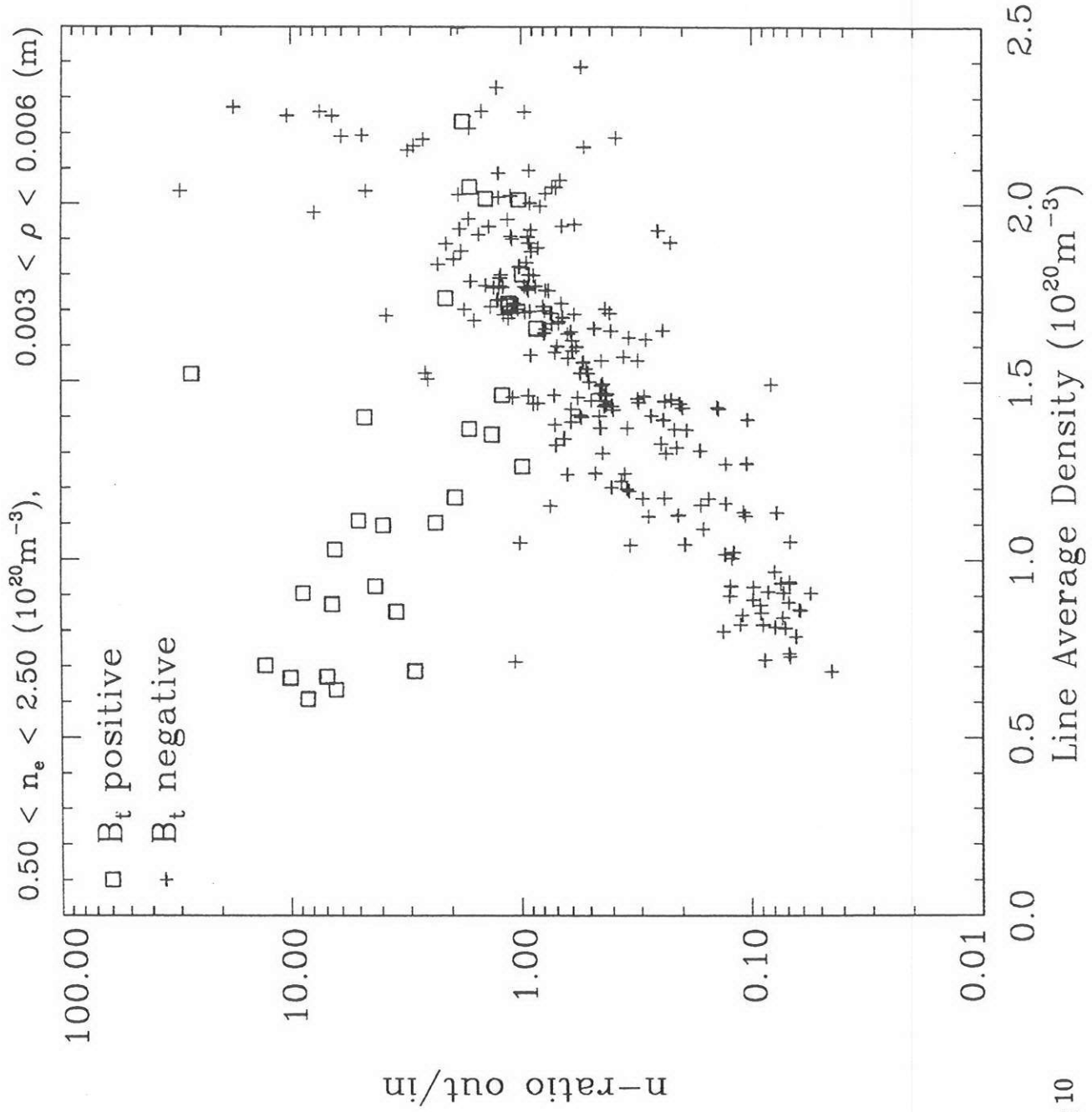
Fig 10
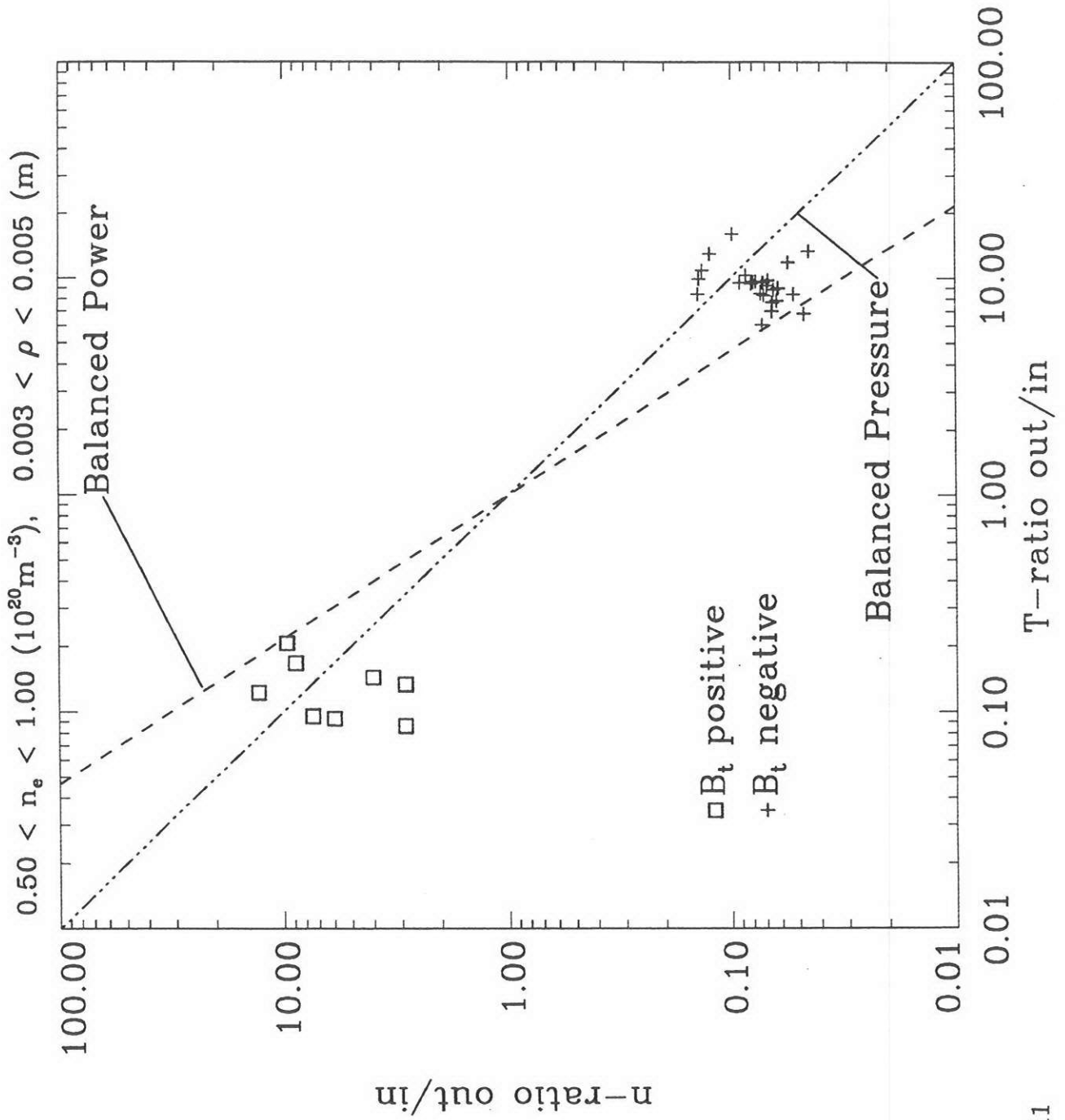
Fig 11

Fig 12

Negative Toroidal Field

Fig 13